EEET ECOLOGICAL ENGINEERING & ENVIRONMENTAL TECHNOLOGY

Ecological Engineering & Environmental Technology, 2025, 26(10), 74–85
https://doi.org/10.12912/27197050/210101
ISSN 2719–7050, License CC-BY 4.0

Received: 2025.08.17
Accepted: 2025.09.15
Published: 2025.10.01

Spatio-temporal analysis of land surface temperature and biomass changes in Nusantara Capital City: Challenges for forest city planning

Siti Badriyah Rushayati[1*], Lilik Budi Prasetyo[1], Theresa Vindri Pramesti[1], Frandy Halim Wijaya[1], Arif Kurnia Wijayanto[1]

[1] Department of Forest Resources Conservation and Ecotourism, Faculty of Forestry and Environment, IPB University (Bogor Agricultural University), Bogor, Indonesia
* Corresponding author's e-mail: rushayati@apps.ipb.ac.id

ABSTRACT

The development of the Nusantara Capital City (Ibu Kota Nusantara – IKN) in East Kalimantan, Indonesia, poses significant challenges to local climate stability due to rapid changes in land cover. This study aimed to analyse the spatiotemporal patterns of land cover change and the resulting thermal dynamics driven by IKN development using remote sensing data and GIS-based spatial mapping. Landsat 8/OLI imagery from 2018 and 2022 was used to classify land cover, estimate biomass using the global ecosystem dynamics investigation (GEDI) dataset, and calculate land surface temperature (LST) and urban heat island (UHI) intensity. Research findings indicate that from 2018 to 2022, land cover in the Nusantara Capital City changed, with vegetated areas decreasing. The rapid development of IKN caused the average biomass in these areas to decline from 74.25 Mg/ha in 2019 to 66.21 Mg/ha in 2022. Meanwhile, built-up and open land areas increased. Analysis linking land cover changes to LST revealed a direct correlation, where the shift in land cover contributed to a rise in LST. Consequently, between 2018 and 2022, the UHI intensity rose from 0.05 to 0.08, indicating a shift from a very weak to a weak heat island effect. These outcomes highlight the urgent need for strategic management and expansion of vegetated areas to mitigate urban heat and bolster climate resilience.

Keywords: land surface temperature, Nusantara Capital City, urban heat island.

INTRODUCTION

In 2019, the Government of the Republic of Indonesia formally declared its intention to relocate the national capital from DKI Jakarta Province to Nusantara Capital City (Ibu Kota Nusantara – IKN), situated in East Kalimantan Province, specifically within the regencies of Kutai Kartanegara and North Penajam Paser. This relocation strategy aims to address regional disparities, promote equitable development, and alleviate the pressure on Jakarta, in particular, and the island of Java more broadly (Rifaid et al., 2023).

The development of IKN represents a national megaproject that is transforming the landscape of East Kalimantan into a contemporary administrative centre. This developmental initiative has resulted in substantial alterations in large-scale land use and land cover (LULC), notably the conversion of vegetation area into built-up areas and open land to accommodate infrastructure requirements, including roads, buildings, bridges, and other public facilities (Zhang et al., 2025).

Building new infrastructure often reduces vegetation areas, which lowers their biomass (Karakosta and Papathanasiou, 2025). The biomass in these areas is important for capturing carbon through photosynthesis. This helps reduce greenhouse gases like CO_2 and creates a better urban climate over time. But when green spaces are turned into buildings, their important role is at risk.

Changes in land cover can cause an increase in land surface temperatures (LST), which in turn contributes to the formation and intensification of urban heat islands (UHII) (de Almeida, 2021). UHII is defined as the average difference in LST between urban built environments and surrounding non-urban vegetated areas (Jain et al., 2020). Urban regions are dominated by buildings and infrastructure, whereas non-urban areas typically consist of vegetation.

The likelihood of UHI formation and the escalation of UHII is greater in areas undergoing development than in their surrounding regions. To mitigate the emergence of UHI, the establishment of green open spaces is imperative, as they significantly contribute to microclimate regulation by diminishing the urban heat island effect, enhancing thermal comfort, and bolstering climate resilience. Consequently, it is essential to incorporate sustainable urban development strategies by expanding green and open spaces (Liao et al., 2021; Wang et al., 2025).

Uncontrolled city growth that takes over vegetated areas harms local climates and ecosystems in many cities worldwide (Estrada and Perron, 2021; Samat et al., 2020; Zhuang et al., 2022). Cities like Beijing, Islamabad, and Bangkok show that when cities grow without control and reduce vegetated areas, it often leads to higher LST and UHI effects, which harm the environment and public health (Ramsay et al., 2023). As cities expand quickly without planning, they often replace natural areas with concrete and asphalt (Ghosh and Das, 2018; Şahin et al., 2025). This change affects the energy balance of surfaces, raising LST and making UHI effects worse. Losing vegetated areas reduces natural cooling, while more heat-absorbing materials increase heat in cities. These changes cause more than just higher temperatures. Stronger UHI effects can lead to many environmental and health problems. This highlights the need for green infrastructure and sustainable city planning to reduce the negative effects of urban growth on the environment and human health.

The development of IKN adopts a "forest city" concept that integrates sustainable growth while maintaining an ecosystem balance. The city is built in and around forested areas, where forests are planned to cover 70% of the city area. Although IKN follows the forest city concept, as the future capital, urbanisation and expansion will inevitably occur, resulting in population growth and changes in land cover (Pan et al., 2024). This will increase land demand and drive land conversion from vegetated areas to built-up areas and open land. Urbanisation and population growth will also trigger increased emissions from various anthropogenic activities, leading to air pollution and greenhouse gas emissions. Coupled with the decline in green open spaces and the expansion of built-up areas, these changes can result in increased LST and urban heat island effects (Venter et al. 2023).

Although many studies have investigated the dynamics of LST and UHII driven by LULC changes in major cities, there remains a critical information gap regarding how these processes unfold in a newly developing capital city, especially in tropical forest regions such as East Kalimantan, Indonesia. Most previous studies have focused on mature areas. However, there is still a lack of information on how early stage infrastructure development affects the thermal environment in areas designated for future urbanisation. Moreover, very few studies have quantitatively evaluated the rate and extent of LST increases in response to land cover changes during the initial development phase of a national capital city. By assessing early changes in land cover and LST, it is possible to anticipate potential negative impacts. This study is expected to contribute to the realisation of the forest city concept in IKN development. In light of these considerations, this research aims to analyse, in an integrated manner, the spatiotemporal patterns of land cover change and the resulting thermal dynamics driven by IKN development.

MATERIAL AND METHODS

To analyse land cover changes in IKN, East Kalimantan Province, Landsat 8/OLI satellite imagery was used. Data were acquired for two different periods: 1 January to 31 December 2018 and 1 January to 31 December, 2022. To complement the satellite imagery, additional datasets were utilised, including land cover reference data, administrative boundaries, and demographic data provided by the local government.

Data processing and analysis were performed using Google Earth Engine (GEE), ArcGIS Desktop 10.8, and Microsoft Excel. The location of the study is illustrated in Figure 1. This research consisted of several steps:

1. Image composition: merging all available spectral bands using the Composite Bands tool in ArcGIS Desktop 10.5;
2. Image projection: transforming the coordinate system of the images to the UTM zone 50S;
3. Cloud removal: eliminating clouds and their shadows by utilizing the BQA band from Landsat 8/OLI data, following the method described by Nguyen et al. (2020);
4. Scene mosaicking: combining neighboring scenes to produce a continuous mosaic that covers the entire study region;
5. Masking: cropping the mosaic to fit the administrative borders of the research area;
6. Calculating the normalized difference vegetation index (NDVI);
7. Identifying land cover types; viii) Estimating LST.

Data analysis

The data collection process started with downloading satellite images from the United States Geological Survey (USGS) through the EarthExplorer platform (earthexplorer.usgs.gov). This included Landsat 7/Enhanced Thematic Mapper (ETM) images from 2011 and 2012, as well as Landsat 8/Operational Land Imager (OLI) images from 2013 to 2024. Prior to analysis, gaps in the SLC-off data from Landsat 7/ETM were filled using band-specific gap masks in QGIS. Both Landsat 7 and 8 datasets were utilized to compute LST, net primary productivity (NPP), and fractional cover density (FCD). In contrast, Landsat 5/Thematic Mapper (TM) data was applied for land cover classification but was processed directly within Google Earth Engine (GEE) rather than being downloaded.

Land cover change analysis

Land cover classification was performed using a supervised maximum likelihood method. Training sites corresponding to different land cover types were selected based on their spectral characteristics and visual assessment. The classification scheme applied in this research followed the system introduced by Anderson et al. (1976). The land cover categories identified comprised water bodies, built-up areas, open land, trees, and non-tree vegetation.

To assess the accuracy of the land cover classification, a stratified random sampling approach was used to select 200 sample points from each land cover category. The classified land cover was then compared to ground-truth reference data using a confusion matrix, based on the method outlined by Congalton and Green (2008). According to Lillesand et al. (1979), a classification accuracy of at least 85% is considered satisfactory for remote sensing applications.

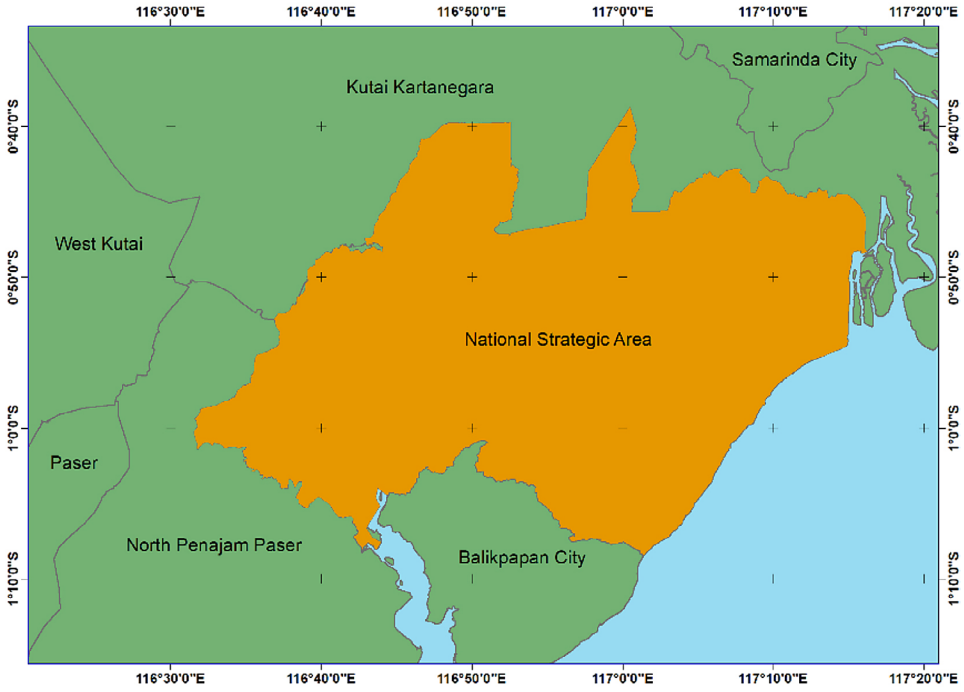

Figure 1. Strategic area in the Nusantara Capital City

A supervised classification method utilizing the maximum likelihood algorithm was used for land cover classification, dividing land use into 12 categories: dry land forest, mangrove forest, swamp forest, plantation forest, built-up land, open land, dry land farming, rice field, bush, and pond. This algorithm classifies pixels as specific objects based on the sample's shape, size, and orientation within the feature space, using ArcGIS software.
The research was conducted in several phases:

- image cropping was performed by executing commands on GEE for the years 2018 and 2022;
- supervised classification involved selecting 200 sample points to represent pixels for each land cover category;
- the transformation of classified raster data into vector data was done using ArcMap 10.8 to determine the area of land cover change from the classified images;
- calculation of land cover area;
- analysis of changes in land cover area.

Above ground biomass

The estimation of biomass was obtained from the Global Ecosystem Dynamics Investigation (GEDI) level 4A biomass dataset. The GEDI data underwent filtering through the Google Earth Engine. Biomass data from 2019 to 2022 were utilized on a monthly basis, depending on data availability. Since only biomass data was needed, the AGBD band was exclusively used. The GEDI biomass data is derived from LiDAR measurements taken from space by the GEDI instrument aboard the International Space Station (ISS). Biomass estimates in the GEDI dataset are generated using models and algorithms developed by Dubayah et al. (2021). The raw LiDAR waveforms collected by GEDI are processed into relative height (RH) metrics, which are stored in the Level 2A (L2A) dataset. These RH metrics act as inputs for biomass estimation models that have been calibrated across various global regions and plant functional types (PFTs). The models then produce estimates of aboveground biomass density (AGBD), which are made available in the Level 4A (L4A) dataset.

Land surface temperature

Top of atmosphere (TOA) radiometric correction – the surface temperature was calculated by converting pixel values, initially in the form of digital numbers (DN), into radiant values using QGIS 3.36. The initial phase of processing satellite images involves radiometric correction, which includes making adjustments to improve the contrast of each pixel, thereby ensuring that the data captured accurately represents real-world conditions (Richards 1986). This process aims to remove disruptions caused by errors in the sensor's optical system, atmospheric influences, and changes in the sun's elevation angle (Jenerowicz et al., 2023). For Landsat 8 imagery, radiometric correction was performed using the raster calculator tool in QGIS 3.36, following the method described by Barsi et al. (2014), as illustrated in Equation 1.

$$L\lambda = MLQcal + AL \tag{1}$$

where: $L\lambda$ – Radiance spectral TOA (watts/m^2 Srad μm), ML – (Radiance_mult_band x), x band 10 and band 11 (Landsat 8/OLI), AL – (Radiance_add_band x), x = band 10 and band 11 (Landsat 8/OLI),
$Qcal$ – uantized and calibrated pixel values (Digital Number).

Temperature brightness

Brightness temperature refers to the microwave radiation emitted from the upper layers of the Earth's atmosphere (Grankov et al., 2017). It is calculated using the spectral radiation values derived from digital numbers. Brightness temperature serves as an indicator for estimating the surface temperature (Ali et al., 2023). This radiation value was subsequently converted from the Kelvin scale to the Celsius scale. The calculation of brightness temperature utilised band 10 from the Landsat 8 image, processed with the raster calculator tool in QGIS 3.36. The conversion from spectral radiation to temperature follows the equation presented in Equation 2, based on the USGS (2019) method.

$$T_b = \left(\frac{K_2}{\ln\left(\frac{K_1}{L_\lambda} + 1\right)} \right) - 273.15 \tag{2}$$

where: Tb – Temperature brightness (°C),
$K1$ – Calibration constant 1, $K2$ – Calibration constant 2, $L\lambda$ – Radiance spectral TOA (watts/m2 Srad μm).

Normalized difference vegetation index

The normalized difference vegetation index (NDVI) is a measure of vegetation greenness

obtained through the digital analysis of satellite sensor brightness data. In this research, Landsat 8 OLI/TIRS Level 2 data were utilized, focusing on band 4 (RED) and band 5 (NIR), which were combined to calculate the NDVI value. This calculation was executed using the raster calculator tool in QGIS 3.36, adhering to the formula provided by Brewer (2012), as depicted in Equation 3:

$$NDVI = \frac{NIR-RED}{NIR+RED} \quad (3)$$

where: *NDVI* – normalized difference vegetation index, *NIR* – Near Infrared (band 5 Landsat 8), *RED* – Red light radiation from a pixel (band 4 Landsat 8).

Land surface emissivity

To determine land surface emissivity (LSE), it is necessary to obtain the vegetation proportion (Pv) from an image (Rouse et al., 1974). The Pv value was computed using the raster calculator tool available in QGIS 3.36. This computation adheres to the formula provided by the USGS (2016), as outlined in Equation 4:

$$Pv = \left(\frac{NDVI - NDVI_{min}}{NDVI_{max} - NDVI_{min}}\right)^2 \quad (4)$$

where: *Pv* – proportion of vegetation, *NDVI* – normalized difference vegetation index, *NDVImin* – minimum value normalized difference vegetation index, *NDVImax* – maximum value normalized difference vegetation index.

LSE must be calculated to estimate the LST. LSE influences the emission of radiation by a blackbody and determines the efficiency of heat energy transmission to the atmosphere (Avdan and Jovanovska, 2016). It represents the ability to convert thermal or heat energy into radiant energy. The LSE was computed using the raster calculator tool in QGIS 3.36, based on a formula incorporating soil and vegetation emissivity as described by Sobrino et al. (2004), with constants m = 0.004 and n = 0.986, shown in Equation 5:

$$\varepsilon = m\,Pv + n$$
$$\varepsilon = 0.004\,Pv + 0.986 \quad (5)$$

where: ε – ground surface emissivity, Pv – proportion of vegetation.

Land surface temperature:

The surface temperature can be calculated using the thermal bands in Landsat 8 OLI/TIRS Level 2 imagery and converting them to brightness temperature values to obtain the surface temperature. Surface temperature estimation involves determining the spectral radiance and brightness temperature. The LST calculation in band 10 was performed using the raster calculator feature in QGIS 3.36, and the results of both were then averaged using the mean formula. The LST calculation, as presented by USGS (2019), was used to analyse the surface temperature, as shown in Equation 6:

$$LST = \frac{Tb}{\left[1 + \left(\frac{\lambda \times Tb}{c2}\right) \times \ln \varepsilon\right]} \quad (6)$$

where: *LST* – land surface temperature, *Tb* – brightness temperature, λ – wavelength of emitted radiance, $c2$ – h × $\frac{c}{s}$ = 1.4388 × 10-2 mK = 14388 μmK, ε = emissivity

The LST values were categorized based on the land cover classes by extracting data points from 100 randomly chosen locations within each class. This procedure was conducted using ArcGIS software. Subsequently, the LST data from 2018 to 2022 were analyzed to assess whether an increase in LST had occurred.

Urban heat island (UHI) intensity

The UHI was calculated to evaluate the thermal effects of urban growth in the IKN region. This index is characterized by the temperature difference between the average LST of urban and non-urban areas, particularly green open spaces (Jain et al., 2020). In this research, urban regions were depicted by built-up land categories, whereas non-urban areas (green open spaces) were defined as regions with vegetation. The average LST for each type of land cover was derived from classified Landsat 8 images for the years 2018 and 2022. The UHI intensity was subsequently determined for both years to assess the rise in LST from 2018 (prior to development) to 2022 (during ongoing development).

The UHI intensity was calculated using the equation proposed by Xu et al. (2013) as follows:

$$TR = (T1 - TA)/TA \quad (7)$$

where: *TR* denotes the relative surface temperature, *TI* stands for the LST measured in the urban core, and *TA* indicates the LST in the surrounding peripheral area – this defines the UHI intensity classification as shown in Table 1.

RESULT AND DISCUSSION

Land cover changes

Between 2018 and 2022, notable changes in land cover occurred. In 2018, before the development of the IKN began, built-up areas covered 10,732.2 hectares, which increased to 11,626.8 hectares by 2022. Starting in 2019, with the commencement of IKN construction, extensive land clearing took place to prepare the infrastructure, including roads, public facilities, office buildings, and housing for officials. This led to an increase in open land from 13,112.9 hectares in 2018 to 16,858.9 hectares in 2022. Vegetation area decreased from 226,548.8 hectares in 2018 to 222,457.7 hectares in 2022. Water bodies also reduced in size from 5,148.1 hectares to 4,678.2 hectares during the same period. Overall, built-up and open land areas expanded, while vegetation and water bodies declined. Land cover maps from 2018 and 2022 are displayed in Figures 2 and 3, with details of land cover change presented in Figure 4 and Table 2.

Ecosystem dynamic investigation

The Global ecosystem dynamics investigation (GEDI) analysis was initiated in 2018, with data becoming accessible in 2019. Consequently, it cannot be utilized to describe biomass conditions prior to the establishment of the IKN, but it is useful for examining the initial phases of development. According to the GEDI analysis, the average biomass in the IKN region at the start of development was 74.25 megagrams per hectare. This figure rose to 85.98 Mg/ha in 2020, then slightly declined to 82.17 Mg/ha in 2021, and experienced a sharp drop to 66.21 Mg/ha in 2022. This notable reduction in biomass was attributed to extensive development, especially in the core area of IKN's government center. The changes in biomass in IKN from 2019 to 2022 are illustrated in Figure 5.

Table 1. Description of the UHI intensity classes

Relative brightness temperature (TR)	UHI intensity class
−0.02 < TR≤0.07	Very weak heat island
0.07< TR≤0.10	Weak heat island
0.10< TR≤0.15	Moderate heat island
0.15< TR≤0.20	Strong heat island
0.20< TR≤0.40	Very strong heat island

Land surface temperature

The spatial analysis results of LST indicated an increase across all types of land cover from 2018 to 2022. In 2018, the LST for different land cover classes ranged between 27.63 °C and 29.50 °C. By 2022, these temperatures rose to a range of 30.95 °C to 34.08 °C. This rise in LST was attributed to the reduction of vegetated areas and the expansion of built-up and open lands, leading to higher temperatures across all land cover classes in 2022. This suggests that physical development directly contributes to the rise in local temperatures. The observed trend highlights the inverse relationship between vegetation cover and LST: areas with more vegetation tend to have lower LST values (Marando et al., 2022; Saha et al., 2024). The spatial distribution of LST in the IKN for the years 2018 and 2022 is illustrated in Figures 6 and 7, while Figure 8 presents the average LST corresponding to each land cover category for those years.

The core urban area, represented by built-up land, corresponds to the highest land surface temperature, while the surrounding peripheral region, primarily covered by vegetation, exhibits lower LST values. UHI increased from 0.05 in 2018 to 0.08 in 2022, indicating a shift from a very weak to a weak heat island effect. This increase in UHII is illustrated in Figure 9.

The increase in UHI from 2018 to 2022 suggests that, despite the development of IKN still being in its early stages, it has already significantly intensified the UHI (Fajary et al., 2024). If this issue is not addressed in urban management, it will hinder the achievement of IKN's vision as a forest city. Without ecological mitigation, the continued development of IKN could lead to the following:

1. A sustained rise in LST
2. The formation of UHI, which worsens thermal comfort
3. A decline in quality of life

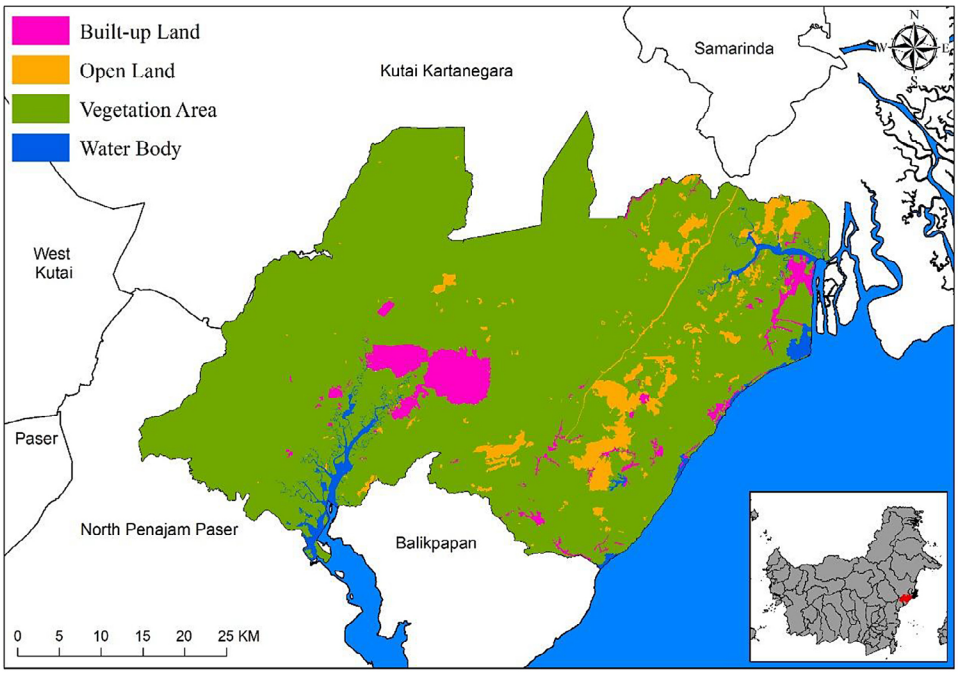

Figure 2. Land cover in the Nusantara Capital City in 2018

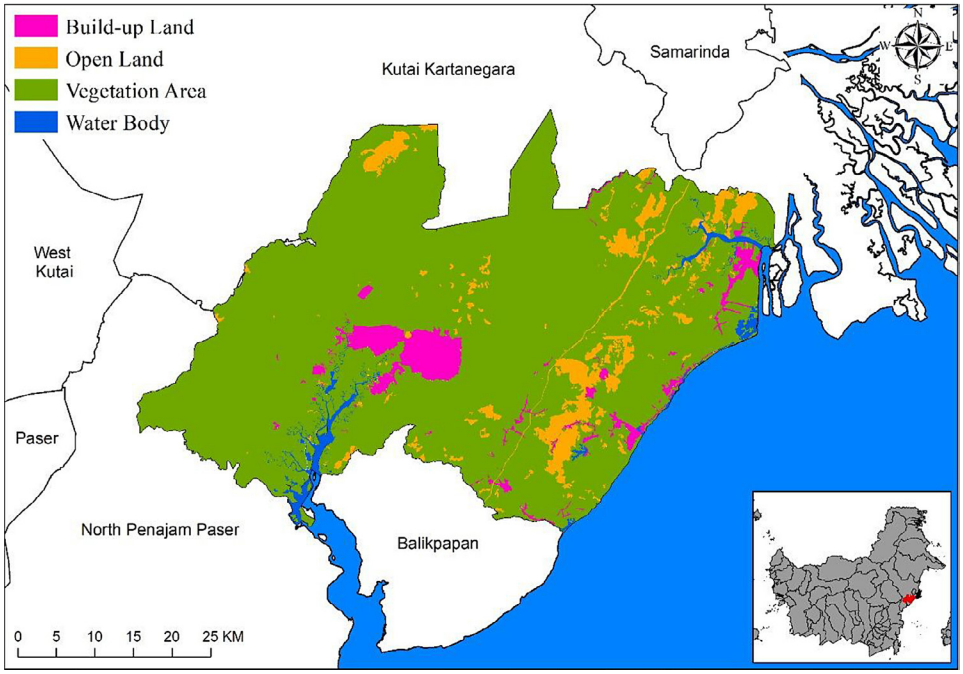

Figure 3. Land cover in the Nusantara Capital City in 2022

4. Hindering the achievement of the IKN development which is based on the forest city concept.

Although IKN adopts the forest city concept, significant increases in LST remain highly likely if land conversion is not controlled holistically. Simply implementing a 70% forest coverage target is insufficient without a strategic spatial approach, thermal landscape design, or long-term monitoring.

Based on the spatial analysis of changes in land use and surface temperature, as well as the UHII assessment, it is evident that although the construction of the IKN is still in early stages and follows the forest city concept, it has already impacted biomass, leading to increased

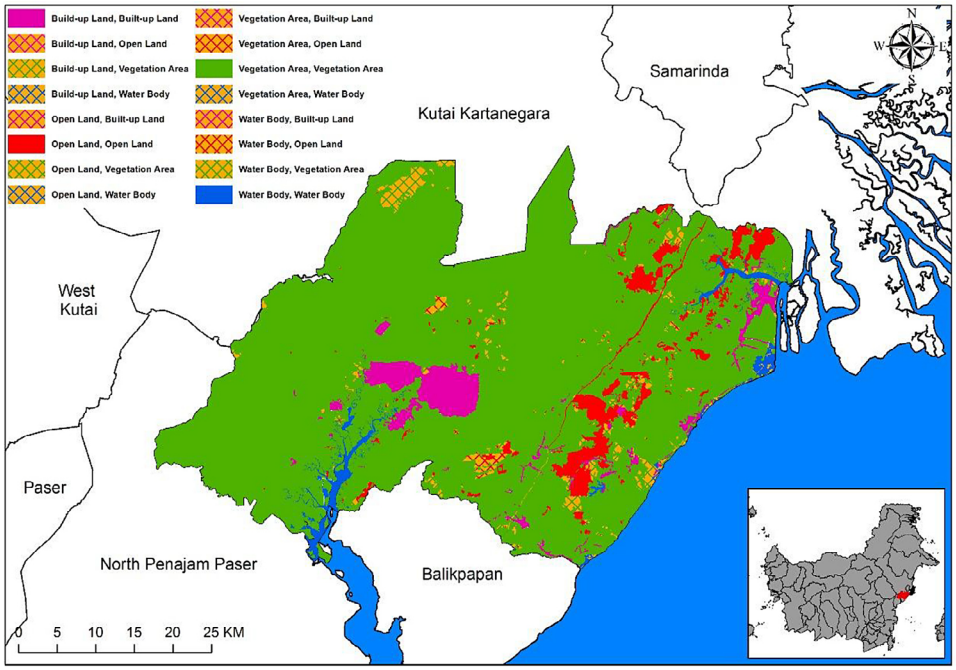

Figure 4. Changes in land cover from 2018 to 2022

Table 2. Changes in land cover of the IKN from 2018 to 2022 (ha)

Year	2022					
2018	Land cover	Built-up land	Open land	Vegetation area	Water body	Total
	Build-up land	10732.2	38.3	85.0	0	10855.5
	Open land	60.5	11615.4	1437.0	0	13112.9
	Vegetation area	784.1	5170.9	220550.1	43.7	226548.8
	Water body	50.0	34.3	385.6	4678.2	5148.1
	Total	11626.8	16858.9	222457.7	4721.9	255665.3

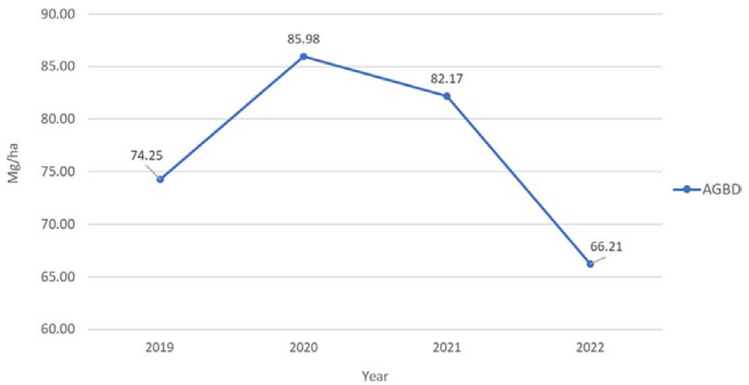

Figure 5. Biomass changes during the development of the Nusantara Capital City

LST and UHII. Continuous monitoring and proactive measures are essential, as the ongoing development may cause further significant rises in these indicators.

The forest city concept aims to maintain a high proportion of vegetation cover to ensure thermal balance, emphasizing not only the amount but also the spatial arrangement, connectivity, and functionality of green areas. These factors are crucial for sustaining ecological balance and mitigating the effects of UHIs. If green spaces are only concentrated on the city's

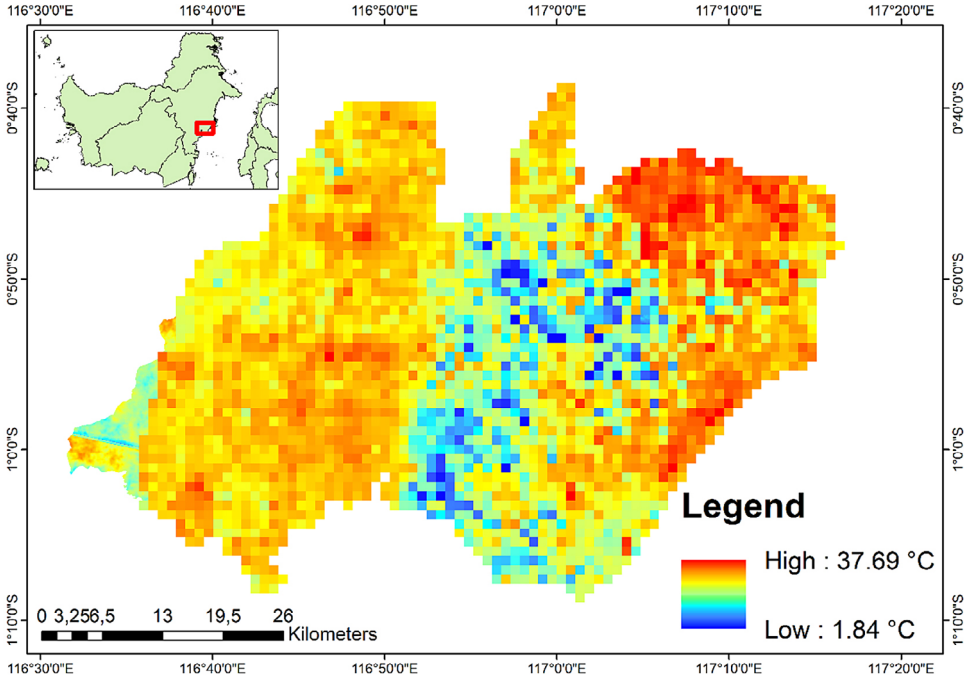

Figure 6. Land surface temperature distribution in in the Nusantara Capital City in 2018

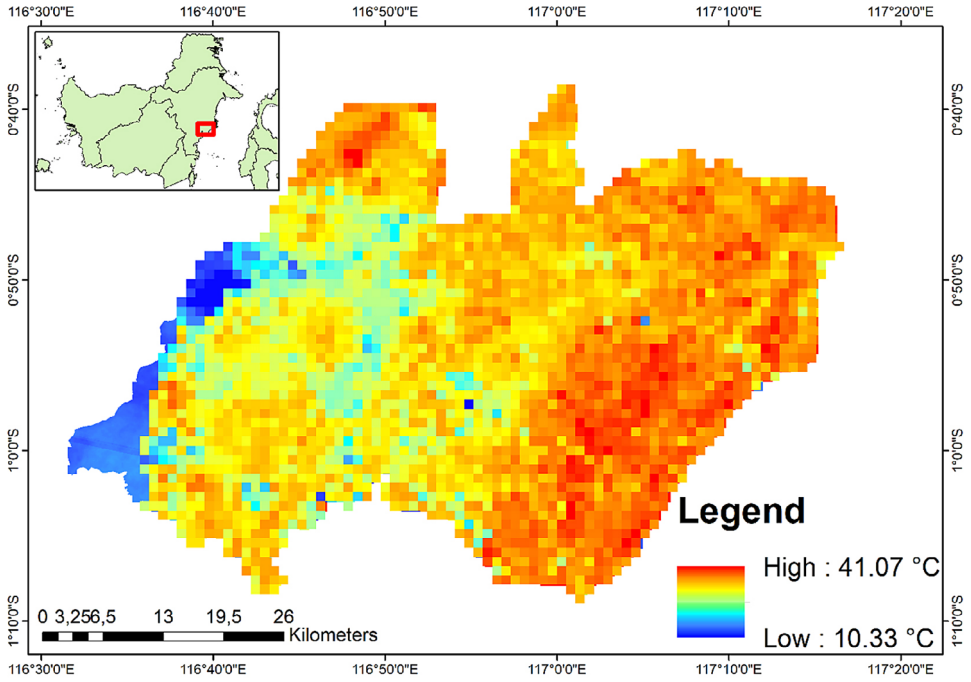

Figure 7. Land surface temperature distribution in Nusantara Capital City in 2022

outskirts without adequate integration into the urban core, the city center remains vulnerable to intense heat and environmental challenges. Therefore, urban planners and policymakers must focus on strategic placement, connectivity, and the role of green spaces within the urban fabric to maximize their cooling benefits.

This study contributes important data and insights to help guide urban management, particularly in implementing forest city principles to counteract the adverse microclimatic effects of large-scale construction, specifically regarding LST and UHII. As the IKN construction continues, biomass is expected to decrease, while LST

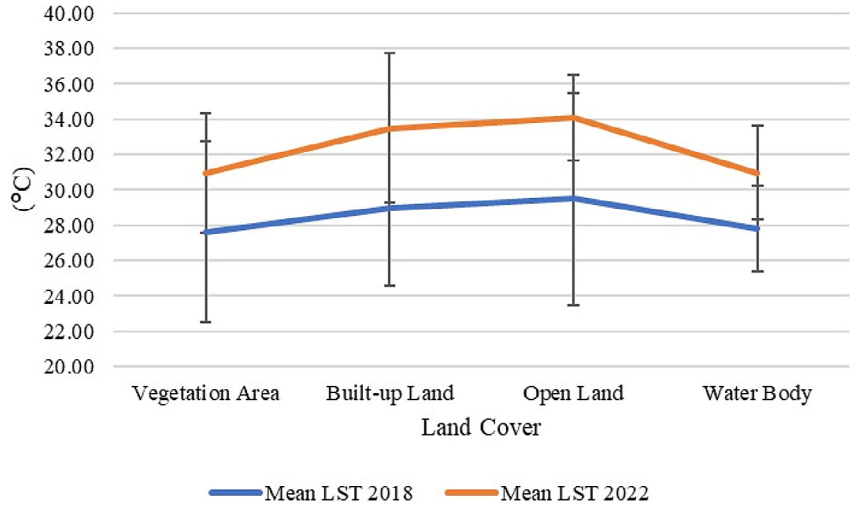

Figure 8. Average LST for each land cover type in 2018 and 2022

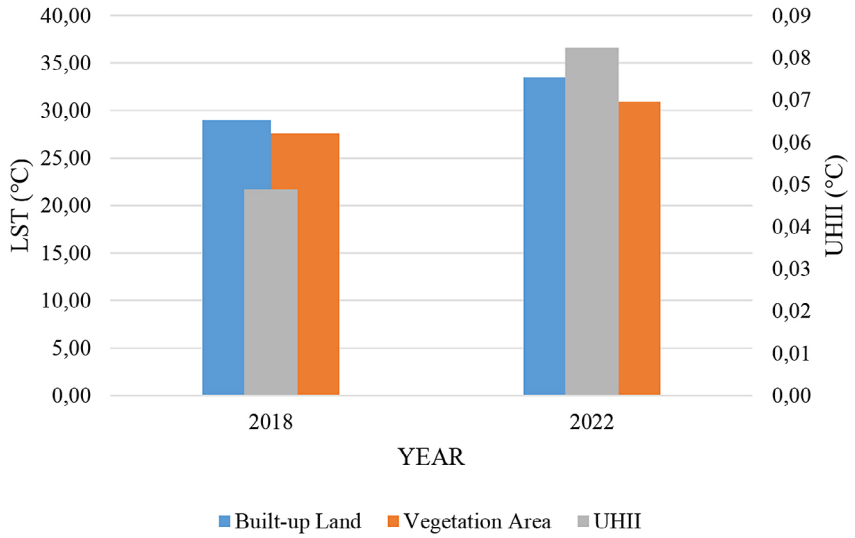

Figure 9. UHI in the Nusantara Capital City in 2018 and 2022

and UHI are expected to rise. Hence, regular monitoring and evaluation by the government are vital to uphold the sustainable development vision of the forest city concept, preserving ecological balance and the city's microclimate.

CONCLUSIONS

This study demonstrated a direct relationship between land cover change, biomass reduction, and increases of LST and UHI intensity in IKN. Land cover changes from 2018 to 2022 contributed to a decline in average biomass owing to the reduction in vegetated areas. The development of IKN has led to a significant increase in surface temperature, as shown by the increase in LST, in line with the transformation of land cover during that period. This increase in the LST has contributed to the increase in the urban heat island intensity. UHI intensity increased from 0.05 in 2018 to 0.08 in 2022, transitioning from a very weak heat island to weak heat island.

These environmental changes must be anticipated through strategic management and the expansion of vegetated land, particularly green open spaces, which are essential for mitigating urban heat and enhancing climate resilience. Furthermore, urban planners should integrate ecological datasets and thermal monitoring into regulations and management practices to ensure the successful realisation of the forest city concept underpinning the development of IKN.

Acknowledgements

We would like to express our gratitude to the Division of Environmental Analysis and Geospatial Modelling, IPB University, and the Ministry of Environment and Forestry for their support in providing the data used in this study.

REFERENCES

1. Ali, S.A., Parvin, F., Ahmad, A. (2023). Retrieval of land surface temperature from landsat 8 oli and tirs: a comparative analysis of radiative transfer equation-based method and split-window algorithm. *Remote Sensing in Earth Systems Sciences*, *6*(1–2). https://doi.org/10.1007/s41976-022-00079-0.
2. Anderson, J.R., Hardy, E.E., Roach, J.T., Witmer, R.E. (1976). A land use and land cover classification system for use with remote sensor data. *U S Geol Surv, Prof Pap*, *964*.
3. Avdan, U., Jovanovska, G. (2016). Algorithm for automated mapping of land surface temperature using LANDSAT 8 satellite data. *Journal of Sensors*, *2016*. https://doi.org/10.1155/2016/1480307
4. Barker, A., Garcia-Blanco, G., Garcia, I., Aguirre-Such, A. (2024). The role of strategic planning in Nature-based Solutions (NBS) transformation: An evaluation of the Green Cities Framework in mainstreaming NBS in 6 European countries. *Nature-Based Solutions*, *6*, 100157.
5. Barsi, J.A., Schott, J.R., Hook, S.J., Raqueno, N.G., Markham, B.L., Radocinski, R.G. (2014). Landsat-8 thermal infrared sensor (TIRS) vicarious radiometric calibration. *Remote Sensing*, *6*(11). https://doi.org/10.3390/rs61111607
6. Brewer, T. (2012). Remote sensing of vegetation: principles, techniques and applications. *Soil Use and Management*, *28*(1). https://doi.org/10.1111/j.1475-2743.2011.00383.x
7. Congalton, R. G., Green, K. (2008). Assessing the accuracy of remotely sensed data: Principles and practices, second edition. In *Assessing the Accuracy of Remotely Sensed Data: Principles and Practices, Second Edition*
8. de Almeida, C. R. (2021). Study of the urban heat island (UHI) using remote sensing data/techniques: A systematic review. *Environments - MDPI*, *8*(10). https://doi.org/10.3390/environments8100105
9. Dubayah RO, Armston J, Kellner JR, Duncanson L, Healey SP, Patterson PL, Hancock S, Tang H, Hofton MA, Blair JB, Luthcke SB. (2021). GEDI L4A footprint level aboveground biomass density, Version 1. Oak Ridge: ORNL DAAC. //daac.ornl.gov/GEDI/guides/GEDI_L4A_AGB_Density.html
10. Estrada, F., Perron, P. (2021). Disentangling the trend in the warming of urban areas into global and local factors. *Annals of the New York Academy of Sciences*, *1504*(1). https://doi.org/10.1111/nyas.14691
11. Fajary, F.R., Lee, H.S., Kubota, T., Bhanage, V., Pradana, R.P., Nimiya, H., Putra, I.D.G.A. (2024). Comprehensive spatiotemporal evaluation of urban growth, surface urban heat island, and urban thermal conditions on Java island of Indonesia and implications for urban planning. *Heliyon*, *10*(13).
12. Ghosh, S., Das, A. (2018). Modelling urban cooling island impact of green space and water bodies on surface urban heat island in a continuously developing urban area. *Modeling Earth Systems and Environment*, *4*(2). https://doi.org/10.1007/s40808-018-0456-7
13. Grankov, A.G., Mil'shin, A.A., Shelobanova, N.K. (2017). Brightness temperature of microwave self-radiation employed as direct characteristic of the dynamic interaction between the ocean and atmosphere. *Journal of Communications Technology and Electronics*, *62*(1). https://doi.org/10.1134/S1064226917010065
14. Jain, S., Sannigrahi, S., Sen, S., Bhatt, S., Chakraborti, S., Rahmat, S. (2020). Urban heat island intensity and its mitigation strategies in the fast-growing urban area. *Journal of Urban Management*, *9*(1). https://doi.org/10.1016/j.jum.2019.09.004
15. Jenerowicz, A., Wierzbicki, D., Kedzierski, M. (2023). Radiometric correction with topography influence of multispectral imagery obtained from unmanned aerial vehicles. *Remote Sensing*, *15*(8). https://doi.org/10.3390/rs15082059
16. Karakosta, C., Papathanasiou, J. (2025). Decarbonizing the construction sector: strategies and pathways for greenhouse gas emissions reduction. In *Energies 18*(5). https://doi.org/10.3390/en18051285
17. Liao, W., Cai, Z., Feng, Y., Gan, D., Li, X. (2021). A simple and easy method to quantify the cool island intensity of urban greenspace. *Urban Forestry and Urban Greening*, *62*. https://doi.org/10.1016/j.ufug.2021.127173
18. Lillesand, T.M., Kiefer, R.W. (1979). Remote sensing and image interpretation. *Remote Sensing and Image Interpretation.* https://doi.org/10.2307/634969
19. Marando, F., Heris, M.P., Zulian, G., Udías, A., Mentaschi, L., Chrysoulakis, N., Parastatidis, D., Maes, J. (2022). Urban heat island mitigation by green infrastructure in European Functional Urban Areas. *Sustainable Cities and Society*, *77*, 103564.
20. Nguyen, M.D., Baez-Villanueva, O. M., Bui, D.D., Nguyen, P.T., Ribbe, L. (2020). Harmonization of landsat and sentinel 2 for crop monitoring in drought prone areas: Case studies of Ninh Thuan (Vietnam) and Bekaa (Lebanon). *Remote Sensing*, *12*(2), 1–18.

https://doi.org/10.3390/rs12020281

21. Pan, Y., Teng, T., Wang, S., Wang, T. (2024). Impact and mechanism of urbanization on urban green development in the Yangtze River Economic Belt. *Ecological Indicators*, *158*, 111612.
22. Ramsay, E.E., Duffy, G.A., Burge, K., Taruc, R.R., Fleming, G.M., Faber, P.A., Chown, S.L. (2023). Spatio-temporal development of the urban heat island in a socioeconomically diverse tropical city. *Environmental Pollution*, *316*, 120443.
23. Richards, J.A. (1986). Error correction and registration of image data. In *Remote Sensing Digital Image Analysis: An Introduction* 33–68. Springer Berlin Heidelberg. https://doi.org/10.1007/978-3-662-02462-1_2
24. Rifaid, R., Abdurrahman, A., Baharuddin, T., A. Kusuma, B. M. (2023). Smart city development in the new capital city: indonesian government plans. *Journal of Contemporary Governance and Public Policy*, *4*(2). https://doi.org/10.46507/jcgpp.v4i2.141
25. Rouse, J.W., Hass, R.H., Schell, J.A., Deering, D.W., Harlan, J.C. (1974). Monitoring the vernal advancement and retrogradation (green wave effect) of natural vegetation. *Final Report, RSC 1978-4, Texas A & M University, College Station, Texas.*
26. Saha, J., Ria, S.S., Sultana, J., Shima, U.A., Hasan Seyam, M.M., Rahman, M.M. (2024). Assessing seasonal dynamics of land surface temperature (LST) and land use land cover (LULC) in Bhairab, Kishoreganj, Bangladesh: A geospatial analysis from 2008 to 2023. *Case Studies in Chemical and Environmental Engineering*, *9*. https://doi.org/10.1016/j.cscee.2023.100560
27. Şahin, M.T., Hadimli, H., Çakır, Ç., Yasak, Ü., Genişyürek, F. (2025). The role of urban landscape on land surface temperature: the case of Muratpaşa, Antalya. *Land*, *14*(4). https://doi.org/10.3390/land14040663
28. Samat, N., Mahamud, M.A., Tan, M.L., Tilaki, M.J.M., Tew, Y.L. (2020). Modelling land cover changes in peri-urban areas: A case study of george town conurbation, malaysia. *Land*, *9*(10). https://doi.org/10.3390/land9100373
29. Singh, C., Madhavan, M., Arvind, J., Bazaz, A. (2021). Climate change adaptation in Indian cities: a review of existing actions and spaces for triple wins. *Urban Climate*, *36*, 100783
30. Sobrino, J.A., Jiménez-Muñoz, J.C., Paolini, L. (2004). Land surface temperature retrieval from LANDSAT TM 5. *Remote Sensing of Environment*, *90*(4). https://doi.org/10.1016/j.rse.2004.02.00
31. Venter, Z.S., Figari, H., Krange, O., Gundersen, V. (2023). Environmental justice in a very green city: Spatial inequality in exposure to urban nature, air pollution and heat in Oslo, Norway. *Science of The Total Environment*, *858*, 160193.
32. Wang, A., Dai, Y., Zhang, M., Chen, E. (2025). Exploring the cooling intensity of green cover on urban heat island: A case study of nine main urban districts in Chongqing. *Sustainable Cities and Society*, *124*, 106299. https://doi.org/https://doi.org/10.1016/j.scs.2025.106299
33. Xu, L.Y., Xie, X.D., Li, S. (2013). Correlation analysis of the urban heat island effect and the spatial and temporal distribution of atmospheric particulates using TM images in Beijing. *Environmental Pollution*, *178*. https://doi.org/10.1016/j.envpol.2013.03.006
34. Zhang, Q., Guan, Y., Wu, X., Zhang, J., Li, R., Lin, K., Wang, Y. (2025). Revealing the dynamic effects of land cover change on land surface temperature in global major bay areas. *Building and Environment*, *267*, 112266. https://doi.org/https://doi.org/10.1016/j.buildenv.2024.112266
35. Zhuang, H., Chen, G., Yan, Y., Li, B., Zeng, L., Ou, J., Liu, K., Liu, X. (2022). Simulation of urban land expansion in China at 30 m resolution through 2050 under shared socioeconomic pathways. *GIScience and Remote Sensing*, *59*(1). https://doi.org/10.1080/15481603.2022.2110197